Optical-model analysis of $p + {}^{208}Pb$ elastic scattering from 15–1000 MeV*

W. T. H. van Oers, Huang Haw, and N. E. Davison
Cyclotron Laboratory, Department of Physics, University of Manitoba, Winnipeg, Canada

A. Ingemarsson, B. Fagerström, and G. Tibell
The Gustaf Werner Institute, University of Uppsala, Uppsala, Sweden

(Received 4 March 1974)

Measurements have been made of the differential cross sections for $p + {}^{208}Pb$ elastic scattering at mean proton energies of 21.0, 24.1, 26.3, 30.5, 35.0, 45.0, and 47.3 MeV. Measurements have also been made of the differential cross sections and polarizations at 185 MeV. These data together with the data in the energy range 15–1000 MeV available in the literature have been analyzed in terms of a standard 11-parameter optical model. Relativistic corrections to the optical-model analysis were introduced. The energy dependence of the real central potential (as indicated by the volume integral per nucleon and by the strength parameter) can be represented by a linear relation if a limited energy range is chosen. This linear energy relation cannot be extrapolated to higher energies since it makes the real central potential repulsive at too low an energy as indicated by the results of optical-model analyses of proton scattering data above 200 MeV. A logarithmic energy dependence gives a reasonable presentation of the volume integral per nucleon of the real central potential for energies up to 1 GeV.

[NUCLEAR SCATTERING $^{208}Pb(p,p)$, $T = 21.0$, 24.1, 26.3, 30.5, 35.0, 45.0, and 47.3 MeV, measured $\sigma(\theta)$, $\theta = 15$–$167.5°$; $T = 185$ MeV measured $\sigma(\theta)$, $P(\theta)$, $\theta = 4$–$38°$; optical-model analysis, previous data $\sigma(\theta)$, $P(\theta)$, σ^R included.]

INTRODUCTION

The nucleon-nucleus potential which describes the over-all features of the nucleon-nucleus interaction is energy-dependent and nonlocal.[1,2] When a purely nonlocal potential is replaced by an equivalent local potential, the latter will show an energy dependence. Consequently, phenomenological optical-model potentials, which are usually chosen to be local potentials and whose parameters are determined by fitting nucleon-nucleus scattering data, will exhibit an energy dependence which is due in part to the intrinsic energy dependence of the nonlocal optical potential and in part to the nonlocality. The intrinsic energy dependence of the optical potential must be such that the real and imaginary parts satisfy a dispersion relation.[1,3] Studies of the energy dependence of equivalent local optical potentials have been undertaken by Lipperheide and Schmidt[3] and by Fiedeldey and Engelbrecht[4] for the energy range 0–200 MeV and by Passatore[5] for the energy range 10–1000 MeV. Engelbrecht and Fiedeldey calculated the real part of the neutron-nucleus optical potential as the equivalent local potential of an energy-independent real nonlocal potential and a dispersion integral over an energy-dependent imaginary local potential. The equivalent local optical potential gives reasonable agreement with neutron scattering data in the energy range 0–160 MeV. However, the energy dependence of the strength of the real potential has been expressed in a form which cannot be extrapolated to higher energies. Lipperheide and Schmidt used as input for the dispersion integral phenomenological imaginary local potentials, obtained for $p + {}^{12}C$, $p + {}^{40}Ca$, and $p + {}^{58}Ni$ elastic scattering extrapolated linearly to zero at various cutoff energies. The volume integral of the real part of the equivalent local potential when extrapolated to higher energies does not change sign as indicated by higher-energy scattering data. A similar prescription for deriving the equivalent local potential has been followed by Passatore. The phenomenological imaginary local potential that was used as input for the dispersion integral contained a nonzero high-energy limit. Thus a subtracted dispersion relation had to be used which introduced an unknown additive constant contribution to the real potential.

To study in detail the energy dependence of the phenomenological optical potential over a considerable energy range, systematic optical-model analyses have recently been made of the $p + {}^{16}O$ system in the energy range 20–100 MeV[6] and of the $p + {}^{40}Ca$ system in the energy range 10–180 MeV.[7] The present study deals with the $p + {}^{208}Pb$ system for which one may expect that, at least above an incident proton energy $T_p = 20$ MeV, many

of the difficulties encountered in optical-model analyses of proton scattering from the light nuclei are not present, e.g., compound nucleus scattering and resonances in the intermediate compound system. To obtain a consistent set of low-energy $p+^{208}$Pb differential cross-section angular distributions, cross sections were measured at 21.0, 24.1, 26.3, 30.5, 35.0, 45.0, and 47.3 MeV. To complement the higher-energy data measurements were also made of the differential cross sections and

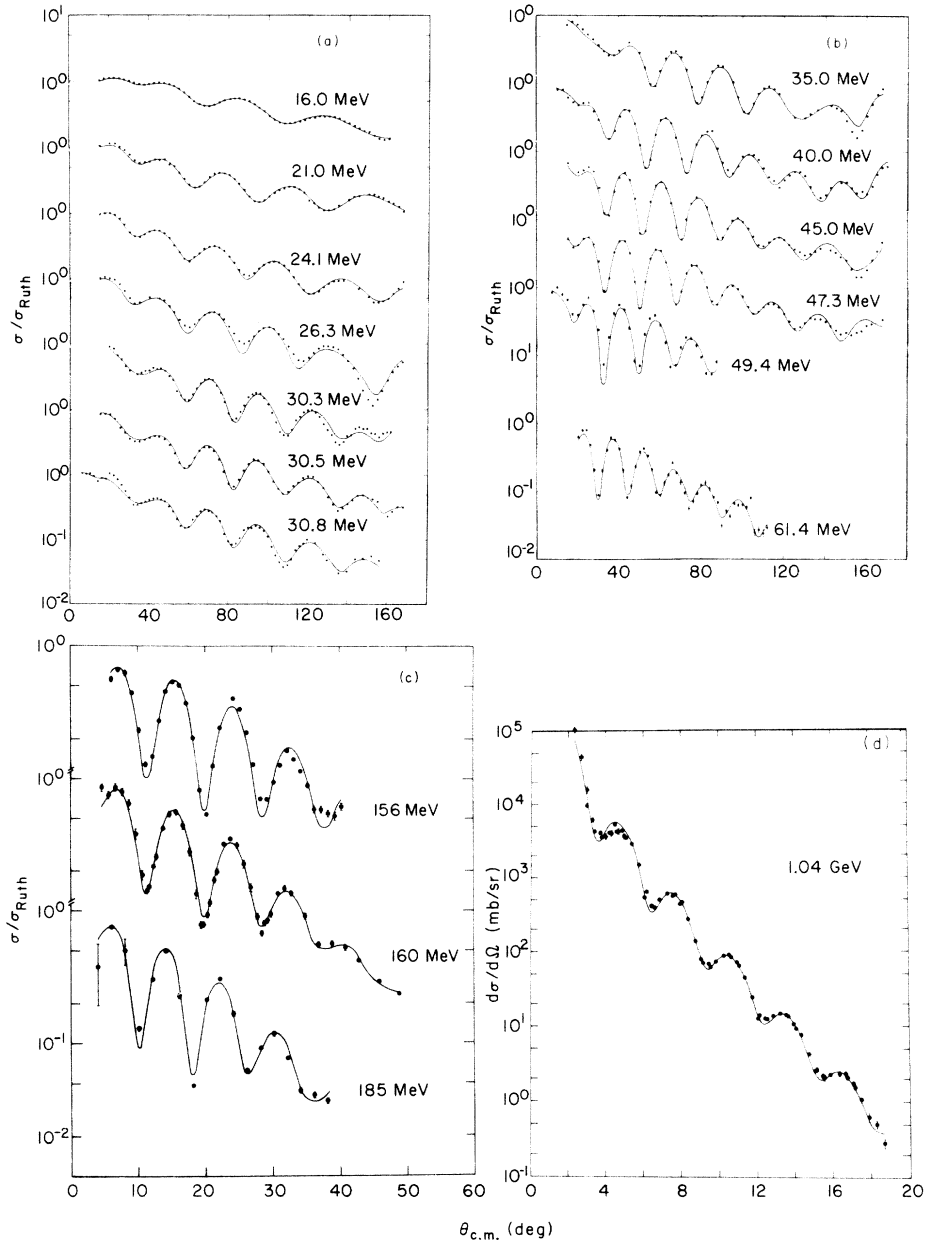

FIG. 1. (a) The differential scattering cross sections divided by the Rutherford cross section for the elastic scattering of protons from ^{208}Pb at 16.0, 21.0, 24.1, 26.3, 30.3, 30.5, and 30.8 MeV. The experimental errors are comparable to the size of the dots unless indicated by error bars. The data selection is indicated in Table I. The solid lines represent the "all parameter" optical-model fits. (b) The differential scattering cross sections divided by the Rutherford cross section for the elastic scattering of protons from ^{208}Pb at 35.0, 40.0, 45.0, 47.3, 49.4, and 61.4 MeV. (c) The differential scattering cross sections divided by the Rutherford cross section for the elastic scattering of protons from ^{208}Pb at 156, 160, and 185 MeV. (d) Fit to the 1.04-GeV $p+^{208}$Pb elastic scattering differential cross sections for a complex central proton-nucleus optical potential.

polarizations at 185 MeV. In a separate experiment $p + {}^{208}$Pb total reaction cross sections were obtained for the energy range 20–50 MeV.[8] These data together with $p + {}^{208}$Pb elastic scattering and total reaction cross-section data from the literature were analyzed in terms of a standard 11-parameter optical model. The analysis was performed using standard nonrelativistic optical-model codes, but relativistic effects were taken into account by a modification of the wave number and corrections to the strengths of the central potentials as discussed in Ref. 9.

MEASUREMENT OF THE DIFFERENTIAL CROSS SECTIONS AT 21.0, 24.1, 26.3, 30.5, 35.0, 45.0, AND 47.3 MeV

Targets enriched to 99.3% in ^{208}Pb and with nominal thicknesses of 5.0 and 10.0 mg cm^{-2} were bombarded with momentum-analyzed proton beams from the University of Manitoba sector-focused cyclotron. The incident proton beams had an energy spread corresponding to about 150 keV [full width at half-maximum (FWHM)] at 50 MeV. The incident proton energies were known with an uncertainty of ±150 keV from a calibration of the bending magnet using cross-over measurements.[10]

The reaction products were observed simultaneously at eight angles using an array of eight NaI(Tl) detector assemblies placed in a crescent shaped box which could be rotated around the center of a 117-cm i.d. scattering chamber. The detector box contains eight interchangeable collimators with apertures 10.00° apart. The accuracy with which the scattering angles could be set was ±0.02°. Since no collimators were used downstream from the momentum analyzing slits, two monitor detectors with closely similar geometries were set at equal angles (15°) left and right of the incident beam. This enabled verification that the incident beam passed along the zero degree axis of the scattering chamber. If the ratio of the number of elastic counts in the two monitor detectors varied from 1.00 by more than 0.03, slight adjust-

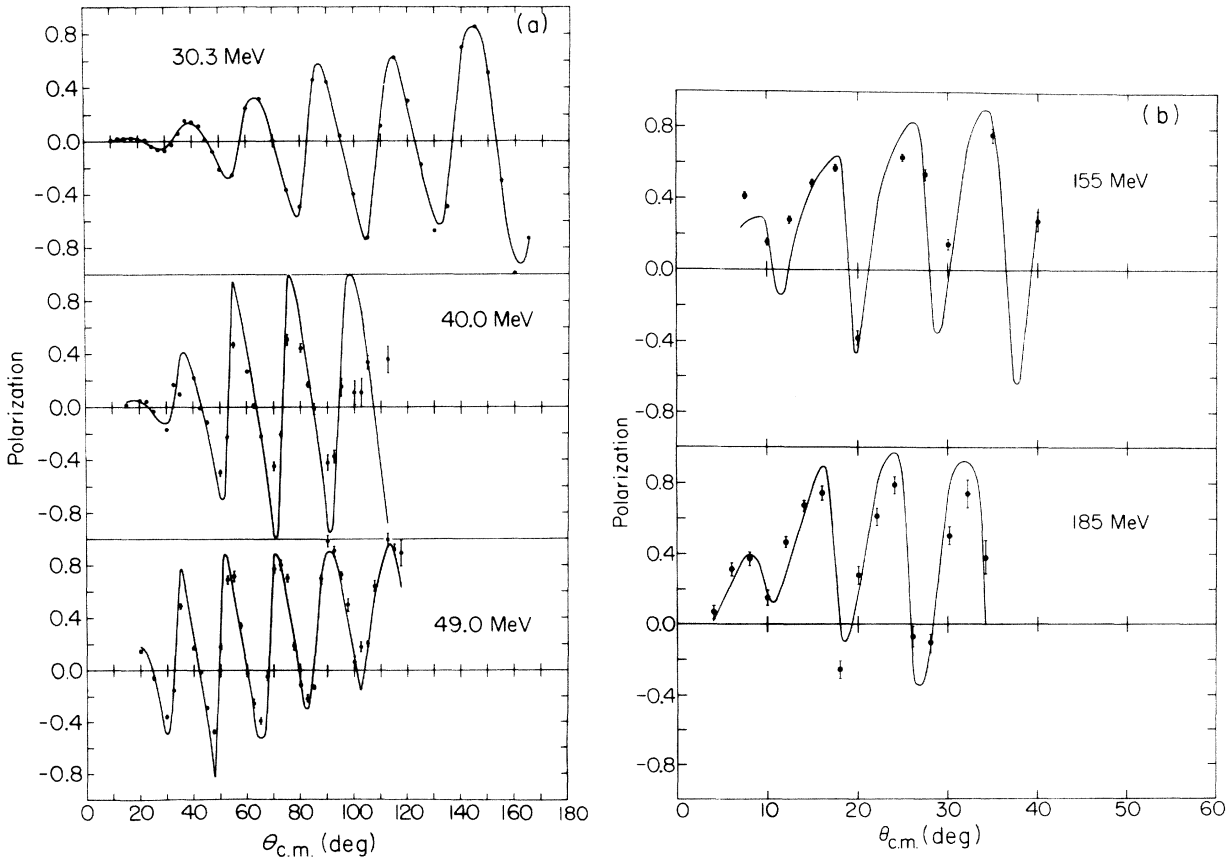

FIG. 2. (a) Polarizations for the elastic scattering of protons from ^{208}Pb at 30.3, 40.0, and 49.0 MeV. The experimental errors are comparable to the size of the dots unless indicated by error bars. The data selection is presented in Table I. The solid lines represent the "all parameter" optical-model fits. (b) Polarizations for the elastic scattering of protons from ^{208}Pb at 155.0 and 185.0 MeV.

ments were made in the beam transport parameters to bring the ratio back to within the allowed limits. Additional checks to verify that the incident beam indeed passed along the zero degree axis of the scattering chamber were made with the multidetector array set alternately left and right of the incident beam. A comparison was then made of the elastic yields at the same scattering angle for closely similar geometries. The differences between the incident beam direction and the zero degree axis were found always to be less than 0.02°.

Two different target positions were used (the angle between a normal to the target and the incident beam direction was either −30° or −150°). The target angle could be set with an accuracy better than ±0.5°. The variation in the target thickness over that part of the target which was illuminated by the incident beam (a typical beamspot was 0.3 cm wide by 0.6 cm high) was determined to be less than 0.8%. The incident beam was collected in a well-shielded Faraday cup and integrated using a current integrator.

The differential cross sections were measured in 2.5° steps between 15 and 167.5°(lab). Two corrections were applied to the data. The first correction takes into account that the measurements were done with a finite solid angle, a beam of finite size at the target, and a beam which in first approximation converges towards the target. The finite geometry correction factor used was taken from Willmes with modifications due to Bray *et al.*[11] The second correction is for the fraction of elastically scattered protons lost due to nuclear reactions in the NaI(Tl) scintillators.[12]

The differential cross sections have relative errors which are in general less than 3%. The relative uncertainties include contributions from: (i) counting statistics, (ii) uncertainties in the electronic deadtime correction (±10% of the correction), (iii) uncertainties in the setting of the target angle (±0.5°), (iv) uncertainties in the setting of the scattering angle (±0.02°), and (v) the relative errors in the solid angle determination. The absolute error in the measurements is estimated to be 3%. The absolute uncertainty includes contributions from: (i) the uncertainty in the target thickness, (ii) the uncertainty in the beam current integration (±1%), (iii) the absolute error in the solid angle determination, (iv) the uncertainty in the direction of the incident beam with respect to the zero degree axis of the scattering chamber (±0.02°), and (v) the uncertainty in the correction for nuclear reactions in the NaI(Tl) scintillators (±20% of the correction). The uncertainty in the incident proton energy was not expressed as an uncertainty in the differential cross sections because of the non-monotonic variation of the angular distributions with energy. The measured differential cross sections are shown in Fig. 1 as ratios to the Rutherford differential cross sections in the center-of-momentum frame. The relative errors are comparable to the size of the dots. Relativistic center-of-momentum transformations were used throughout.

MEASUREMENT OF THE DIFFERENTIAL CROSS SECTIONS AND POLARIZATIONS AT 185 MeV

The 185-MeV data were obtained using the external proton beam of the synchrocyclotron of the Gustaf Werner Institute. An 80-mg cm^{-2}-thick target of ^{208}Pb enriched to 99% was bombarded with the proton beam whose energy spread is less than 200 keV (FWHM). The scattered protons were momentum-analyzed in a magnetic spectrometer with a horizontal opening angle of 1.17° determined by a collimator at the entrance.

In the measurement of the differential cross sections the scattered protons were detected in a scintillation counter hodoscope with 16 energy channels. In the measurement of the polarizations a polarimeter with two independent channels was used. In both experiments the total energy resolution including the energy straggling in the target was less than 300 keV (FWHM). The scattering angle of the protons as fixed by the setting of the spectrometer could be determined to ±0.05°.

Absolute values of the differential cross sections were obtained with the aid of known proton-proton cross sections and a measurement of the scattering from a polyethylene target. The error in the absolute scale which includes the errors in the calibration procedure and the target thickness determination was calculated to be 8.3%.

The absolute scale of the polarization was determined by a measurement of the asymmetry for protons elastically scattered from ^{12}C at 12.5°(lab). The polarization at this scattering angle, 0.769 ± 0.022, is known from a previous measurement.[13] The energy dependence of the analyzing power was determined by placing polythene absorbers in front of the polarimeter. The error in the absolute scale obtained in this manner was determined to be 5%. The measured differential cross sections are shown in Fig. 1 as ratios to the Rutherford differential cross sections in the center-of-momentum frame. The measured polarizations are shown in Fig. 2.

Numerical values of the measured differential cross sections and polarizations can be obtained by request as an addendum to this paper.

TABLE I. Data selection for the $p + {}^{208}Pb$ optical-model analysis in the energy range 15–1000 MeV.

T_p (MeV)	$\sigma(\theta)$ (Ref.)	$P(\theta)$ (Ref.)	σ_T (Ref.)	T_p (MeV)	$\sigma(\theta)$ (Ref.)	$P(\theta)$ (Ref.)	σ_T (Ref.)
16.0	a	···	b	45.0	Present experiment	···	d
21.0	Present experiment	c	d	47.3	Present experiment	···	d
24.1	Present experiment	···	d	49.4	l	m	g
26.3	Present experiment	···	d	61.4	n	···	g
30.3	e	f	d,g	156.0	o	o	p
30.5	Present experiment	f	d,g	160.0	q	···	p
30.8	h	i	d,g	185.0	Present experiment	Present experiment	p
35.0	Present experiment	···	d	1040	r	···	s
40.0	j,g	k	d,g				

[a] Reference 26.
[b] R. E. Pollock and G. Schrank, Phys. Rev. 140, 575 (1965).
[c] E. T. Boschitz, R. W. Bercaw, and J. S. Vincent, Phys. Lett. 13, 322 (1964), data at 18.7 MeV.
[d] Reference 8.
[e] B. W. Ridley and J. F. Turner, Nucl. Phys. 58, 497 (1964).
[f] Reference 24.
[g] J. J. M. Menet, E. E. Gross, J. J. Malanify, and A. Zucker, Phys. Rev. C 4, 1114 (1971).
[h] D. W. Devins, H. H. Forster, and G. G. Grigas, Nucl. Phys. 35, 671 (1962).
[i] R. M. Craig, J. C. Dore, G. W. Greenlees, J. S. Lilley, J. Lowe, and P. C. Rowe, Nucl. Phys. 58, 515 (1964).
[j] L. N. Blumberg, E. E. Gross, A. van der Woude, A. Zucker, and R. H. Bassel, Phys. Rev. 147, 812 (1966).
[k] Reference 19.
[l] G. S. Mani, D. T. Jones, and D. Jacques, Nucl. Phys. A165, 384 (1971).
[m] R. M. Craig, J. C. Dore, J. Lowe, and D. L. Watson, Nucl. Phys. 86, 113 (1966).
[n] C. B. Fulmer, J. B. Ball, A. Scott, and M. L. Whiten, Phys. Rev. 181, 1565 (1969).
[o] A. Willis, B. Geoffrion, N. Marty, M. Morlet, and B. Tatischeff, J. Phys. 30, 13 (1969). New measurements of the 156-MeV differential cross sections have been made recently (V. Comparat, private communication). Consequently only the latter data have been used in the analysis.
[p] Obtained by P. G. Roos and N. S. Wall [Phys. Rev. 140, B1237 (1965)] by extrapolating from the data of A. Johansson, U. Svanberg, and O. Sundberg, Ark. Fys. 19, 527 (1961).
[q] P. G. Roos and N. S. Wall, see footnote p.
[r] R. Bertini, R. Beurtey, F. Brochard, G. Bruge, H. Catz, A. Chameaux, J. M. Durand, J. C. Faivre, J. M. Fontaine, D. Garreta, C. Gustafsson, D. Hendrie, F. Hibou, D. Legrand, J. Saudinos, and J. Thirion, Phys. Lett. 45B, 119 (1973).
[s] Extrapolated to 1.04 GeV from the data of P. U. Renberg, D. F. Measday, M. Pepin, P. Schwaller, B. Favier, and C. Richard-Serre, Nucl. Phys. A183, 81 (1972).

DATA SELECTION

The optical-model analysis includes, in addition to the experimental data obtained in the present experiments and the total reaction cross section data obtained in a separate experiment,[8] the $p + {}^{208}Pb$ elastic scattering and total reaction cross-section data presented in the literature for the energy range 10–1000 MeV. Data sets at 17 energies were analyzed. Ideally each data set should consist of a differential cross-section angular distribution, a polarization angular distribution, and a total reaction cross-section datum. However, polarization angular distributions were available only at seven energies. The data selection is presented in Table I.

The experimental uncertainties used in the definition of χ^2 were the quoted relative errors. The effects of finite angular resolution and the uncertainty in the scattering angle were taken into account only at the higher energies. These effects were found to be nonnegligible in calculating the theoretical polarization angular distributions.

OPTICAL-MODEL ANALYSIS

A. Optical potential

The $p + {}^{208}Pb$ elastic scattering data were analyzed using 11-parameter automatic search codes which are modified and extended versions of the programs SEEK[14] and ELSR.[15] Full details about the method of analysis can be found in Refs. 7 and 16. The optical-model analysis was performed

TABLE II. Optical-model parameters from least-squares searches of p + ^{208}Pb elastic scattering data in the energy range 15–1000 MeV. The quantities N_σ and N_P refer to the number of experimental differential cross sections and polarizations, respectively, while the quantities N_1^{-1} and N_2^{-1} are the normalization factors to the differential cross sections and polarizations, respectively, suggested by the least-squares search. All other quantities are defined in the text. The parameters in parentheses were kept fixed during the search. In the searches done with the optical model code MAGALI (Ref. 36) effects due to the experimental angular resolutions, and the uncertainties in the scattering angle and the absolute normalizations were treated explicitly. Note that in the searches using the optical code MAGALI the imaginary spin-orbit geometry was slightly different from the real spin-orbit geometry.

	T_p (MeV)	V (MeV)	r_0 (fm)	a_0 (fm)	W (MeV)	W_D (MeV)	r_i (fm)	a_i (fm)	V_s (MeV)	W_s (MeV)	r_s (fm)	a_s (fm)
	16.0	51.88	1.327	0.537	(0.0)	21.06	1.191	0.421	(6.04)	(0.0)	(1.064)	(0.738)
	21.0	53.75	1.219	0.743	(0.0)	10.93	1.302	0.654	(6.04)	(0.0)	(1.064)	(0.738)
	24.1	55.12	1.191	0.773	(0.0)	10.30	1.283	0.765	(6.04)	(0.0)	(1.064)	(0.738)
$\theta_{c.m.}<120°$	26.3	55.33	1.177	0.657	(0.0)	9.14	1.262	0.844	(6.04)	(0.0)	(1.064)	(0.738)
	26.3	57.29	1.151	0.757	(0.0)	8.64	1.308	0.838	(6.04)	(0.0)	(1.604)	(0.738)
	30.3	53.07	1.173	0.705	2.22	7.82	1.287	0.750	6.00	(0.0)	1.172	0.603
	30.5	54.63	1.160	0.749	1.82	8.98	1.287	0.750	6.45	(0.0)	1.224	0.571
	30.8	53.71	1.170	0.661	2.47	8.65	1.252	0.773	5.84	(0.0)	1.226	0.514
$\theta_{c.m.}<120°$	35.0	54.62	1.146	0.758	3.00	7.82	1.288	0.696	6.04	(0.0)	(1.064)	(0.738)
	35.0	53.84	1.160	0.739	4.29	6.46	1.286	0.702	6.04	(0.0)	(1.064)	(0.738)
	40.0	51.80	1.159	0.784	3.98	5.75	1.321	0.727	6.66	(0.0)	1.044	0.905
	45.0	50.62	1.156	0.750	4.35	6.00	1.300	0.662	(6.04)	(0.0)	(1.064)	(0.738)
	47.3	48.26	1.183	0.712	4.31	5.74	1.275	0.705	(6.04)	(0.0)	(1.064)	(0.738)
	49.4	47.52	1.168	0.810	4.09	5.51	1.233	0.777	5.93	(0.0)	1.133	0.790
	61.4	46.29	1.173	0.682	3.31	11.50	1.263	0.555	(6.04)	(0.0)	(1.064)	(0.738)
MAGALI	156.0	18.84	1.211	0.663	8.78	(0.0)	1.374	0.457	0.937	−1.742	1.200	0.548
MAGALI	160.0	29.50	1.062	0.791	13.88	(0.0)	1.321	0.546	2.137	−2.008	1.143	0.605
MAGALI	185.0	12.11	1.238	0.836	18.58	(0.0)	1.232	0.642	2.701	−2.96	1.082	0.578
	1040	−8.17	1.125	0.812	28.88	(0.0)	1.117	0.617	(0.0)	(0.0)	(1.090)	(0.620)
	T_p	V	r_0	a_0	W	W_D	r_i	a_i	V_s	r_s	a_s	W_s
MAGALI	156.0	18.86	1.211	0.684	8.74	(0.0)	1.378	0.456	0.819	1.223	0.513	−1.909
MAGALI	160.0	29.58	1.060	0.792	13.91	(0.0)	1.322	0.542	2.067	1.142	0.602	−2.095
MAGALI	185.0	11.63	1.243	0.828	18.87	(0.0)	1.230	0.646	2.797	1.077	0.648	−3.172

using a local potential of the form

$$U(r) = V_C(r) - V\frac{1}{1+\exp(x_1)} - iW\frac{1}{1+\exp(x_2)} + iW_D 4a_i \frac{d}{dr}\left(\frac{1}{1+\exp(x_2)}\right) + (V_s + iW_s)\frac{4}{r}\frac{d}{dr}\left(\frac{1}{1+\exp(x_3)}\right)(\vec{s}\cdot\vec{l}). \quad (1)$$

In this expression $V_C(r)$ denotes the Coulomb potential due to a uniformly charged sphere of total charge Ze and radius R_c where for ^{208}Pb a charge radius $R_c = 1.18A^{1/3}$ fm was used.[17] The quantity V denotes the strength of the real central potential while the quantities W and W_D denote the strengths of the volume and surface parts, respectively, of the imaginary central potential. The quantities V_s and W_s denote the strength of the real and imaginary parts of the spin-orbit potential. The form factors of the real central potential and the volume part of the imaginary central potential are of Woods-Saxon form. The surface part of the imaginary central potential is of a derivative Woods-Saxon form, while the spin-orbit potential is of the usual Thomas type. The remaining factors in the exponential functions contain the radius and diffuseness parameters and are defined as follows:

$$x_1 = \frac{r - r_0 A^{1/3}}{a_0}, \quad x_2 = \frac{r - r_i A^{1/3}}{a_i}, \quad x_3 = \frac{r - r_s A^{1/3}}{a_s}.$$

B. Corrections due to relativistic kinematics

Since relativistic effects in optical-model calculations have been shown to be nonnegligible already at 50 MeV[18] it was found necessary to incorporate relativistic corrections in the present optical-model calculations. As discussed in detail in Ref. 9 there are two main problems. The first one concerns the value of the wave number k which is to be used in the calculations. The second one concerns the correction to be applied to the strengths of the central potential. In the present analysis the wave number has been calculated from the momentum in the center-of-mass sys-

TABLE II *(Continued)*

χ^2_σ	N_σ	N_1	χ^2_P	N_P	N_2	σ_r^{th} (fm^2)	σ_r^{exp} (fm^2)	J/A (MeV fm^3)	$\langle R^2\rangle^{1/2}$ (fm)	γ_{rel}
182.7	59	1.002				94.4	130.0±21.0	531.2	6.41	1.017
228.3	59	1.013				153.2	170.0±10.0	449.3	6.23	1.022
365.8	59	1.013				182.4	186.0±10.0	436.1	6.17	1.025
216.9	41	1.021				188.3	194.0±10.0	411.0	5.93	1.028
3585.	60	1.035				199.0	194.0±10.0	413.4	6.00	1.028
416.0	72	1.007	530.0	40	(1.000)	194.7	211.7± 9.0	395.2	5.99	1.032
1122.	61	0.984	1274.	40	(1.000)	196.8	211.7± 9.0	398.0	6.00	1.032
257.0	67	0.984	178.0	30	(1.000)	193.0	211.7± 9.0	392.7	5.91	1.033
373.7	40	1.025				201.3	204.0±10.0	386.7	5.97	1.037
1852.	57	1.030				199.7	204.0±10.0	389.6	5.98	1.037
1049.	65	0.993	526.2	29	(1.000)	216.9	202.3±10.0	381.2	6.07	1.042
1375.	61	1.036				208.6	200.0±10.0	367.5	5.99	1.048
941.8	62	1.022				209.5	198.0±10.0	373.2	6.07	1.050
463.7	33	1.036	394.5	36	(1.000)	211.5	184.2± 9.5	360.0	6.15	1.052
127.0	47	1.041				207.3	199.3± 9.5	342.7	5.95	1.065
809.3	34	0.988	290.9	11	0.969	170.7	179.0± 5.0	152.0	6.08	1.164
107.1	43	0.992	74.4	16	1.046	189.0	179.0± 5.0	171.1	5.69	1.168
279.3	18	0.935	117.4	16		182.8	179.0± 5.0	108.6	6.48	1.195
397.4	69	1.000				184.9	185.0± 5.0	−116.6	5.97	2.089

r_s	a_s	χ^2_σ	N_σ	N_1	χ^2_P	N_P	N_2	σ_r^{th}	σ_r^{exp}	J/A	$\langle R^2\rangle^{1/2}$	γ_{rel}
1.203	0.574	808.9	34	0.989	283.8	11	0.959	171.4	179.0±5.0	150.3	6.08	1.164
1.145	0.614	104.7	43	0.993	76.0	16	1.043	189.0	179.0±5.0	170.7	5.59	1.168
1.083	0.573	239.5	18	0.952	109.6	16	0.971	182.8	179.0±5.0	105.2	6.48	1.195

tem, given by

$$p' = m_2\left[\frac{T_p(T_p+2m_1)}{(m_1+m_2)^2+2m_2T_p}\right]^{1/2}, \tag{2}$$

where T_p is the kinetic energy of the incident particle in the laboratory system, and m_1 and m_2 are the rest masses of the incident and target particle, respectively. The correction factor γ_{rel}, by which the strengths of the central potential are to be multiplied is obtained from

$$\gamma_{rel} = \frac{p'^2}{E'^2 - m_1^2}\,\frac{E'}{\mu}, \tag{3}$$

where E' is the sum of the kinetic energies in the center-of-mass system and the rest mass of the incident particle and $\mu = m_1m_2/(m_1+m_2)$ is the reduced mass. The central potential strengths presented in Tables II and III have been corrected in this manner. Also included in the tables is the value of γ_{rel} used.

C. Analysis

The first step in the analysis was to find a consistent set of so-called "all parameter" fits. The calculations were performed by searching for best simultaneous fits to both differential cross sections and polarization data (if the latter were available). This was done by minimization of the total χ^2 which is the sum of χ^2 for the differential cross sections and the χ^2 for the polarizations. Initial values for the parameters were taken from various sets of optical-model parameters in the literature. For a fit to be acceptable two additional criteria had to be fulfilled. First it was required that the calculated reaction cross sections agree reasonably well with the experimental reaction cross sections. Second the optical-model parameters found must exhibit a reasonable continuity as a function of incident proton energy. Applying these criteria several fits with smaller values for χ^2 were discarded.

Because a search on the imaginary spin-orbit potential did not lead to an appreciable improve-

TABLE III. Optical-model potential strengths resulting from average geometry least-squares searches to the $p + {}^{208}Pb$ elastic scattering data in the energy range between 15–185 MeV. The parameters in parentheses were kept fixed during the search.

	T_p (MeV)	V (MeV)	W (MeV)	W_D (MeV)	V_s (MeV)	W_s (MeV)	χ^2_σ	N_σ	χ^2_P	N_P	σ_r^{th} (fm^2)	σ_r^{exp} (fm^2)	γ_{rel}
	16.0	61.68	(0.0)	6.28	(6.18)	(0.0)	2759	59			96.7	130.0 ± 21.0	1.017
	21.0	57.30	(0.0)	10.42	(6.18)	(0.0)	313.7	59			148.9	170.0 ± 10.0	1.022
	24.1	56.84	(0.0)	9.65	(6.18)	(0.0)	5019	59			163.5	186.0 ± 10.0	1.025
($\theta_{c.m.}$ <120°)	26.3	54.61	(0.0)	10.51	(6.18)	(0.0)	1575	41			175.6	194.0 ± 10.0	1.028
	26.3	55.97	(0.0)	8.92	(6.18)	(0.0)	20 005	60			170.0	194.0 ± 10.0	1.028
	30.3	52.57	2.96	8.09	5.84	(0.0)	395.5	72	1439	40	189.8	211.7 ± 9.0	1.032
	30.5	53.02	4.48	6.95	5.97	(0.0)	3372	61	1996	40	190.1	211.7 ± 9.0	1.032
	30.8	51.76	3.17	9.12	4.95	(0.0)	409.2	67	321.0	30	194.2	211.7 ± 9.0	1.033
($\theta_{c.m.}$ <120°)	35.0	50.71	2.71	7.87	(6.18)	(0.0)	539.2	40			198.9	204.0 ± 10.0	1.037
	35.0	51.70	5.84	6.00	(6.18)	(0.0)	4361	57			198.0	204.0 ± 10.0	1.037
	40.0	50.54	3.80	7.12	5.87	(0.0)	2023	65	399.2	29	207.2	202.3 ± 10.0	1.042
	45.0	47.23	6.19	4.28	(6.18)	(0.0)	5499	61			205.6	200.0 ± 10.0	1.048
	47.3	48.31	5.90	4.72	(6.18)	(0.0)	3665	62			208.9	198.0 ± 10.0	1.050
	49.4	46.44	7.76	3.20	6.50	(0.0)	423.5	33	541.4	36	206.7	184.2 ± 9.5	1.052
	61.4	44.57	3.75	5.95	(6.18)	(0.0)	316.7	47			210.9	199.3 ± 9.5	1.065
	156.0	17.03	12.06	(0.0)	3.58	−1.31	1746	35	458.9	11	179.3	179.0 ± 5.0	1.164
	160.0	8.63	11.92	(0.0)	3.90	−0.60	809.8	43	83.2	16	176.5	179.0 ± 5.0	1.168
	185.0	10.26	13.33	(0.0)	3.04	−1.60	774.7	18	463.7	16	180.1	179.0 ± 5.0	1.195

ment of the fits to the data, the value of W_s was set equal to zero at all energies except at 156, 160, and 185 MeV. At those energies below 100 MeV where polarization data were not available, the spin-orbit parameters were kept fixed at $V_s = 6.04$ MeV, $r_s = 1.064$ fm, and $a_s = 0.738$ fm. The fixed spin-orbit parameters were adopted from an optical-model analysis by Fricke *et al.*[19] for $A > 28$. These average spin-orbit geometry parameters have been successfully used in the energy range 30–60 MeV. For incident energies below 30 MeV the volume part of the imaginary central potential was set equal to zero, because a search on W gave a small value and no significant improvements to the fits. Similarly the surface part of the imaginary central potential was set equal to zero at the higher energies. The optical-model parameters obtained in the "all parameter" searches and the corresponding theoretical and experimental reaction cross sections are given in Table II.

The theoretical and experimental differential cross-section angular distributions are shown in Fig. 1. In general the quality of the fits is quite good and is certainly much better than for the light nuclei. Some difficulties were encountered at $T_p = 26.3$, 35.0, and to some extent 45.0 MeV where the experimental angular distributions show a pronounced minimum at extreme backward angles which cannot be reproduced by the theoretical calculations. A search over the spin-orbit parameters did not appreciably improve the fits to the backward part of the angular distributions within the range of acceptable values for those parameters. Omitting the differential cross sections for scattering angles $\theta_{c.m.} > 120°$ gave a χ^2 which was smaller by a considerable factor. The results at $T_p = 26.3$ and 35.0 MeV are included in Table II. To ensure that numerical deficiencies were not responsible for the lack of agreement at the extreme backward angles as was pointed out for some ^{3}He-particle optical-model analyses,[20] a study was made of the influence of the following: (i) the step size used in the numerical integration of the wave function, (ii) the number of partial waves used in the expansion of the scattering amplitude, and (iii) the matching point where the external wave functions (a combination of regular and irregular Coulomb wave functions) are matched to the internal wave functions. From this the numerical accuracy of the theoretical angular distributions at $T_p = 26.3$ and 35.0 MeV was estimated to be better than 0.5%. The discrepancies at the extreme backward angles are not unique to the present analysis but have also been found in previous analyses.[7] Similar discrepancies appear even more pronounced in optical-model analyses of the light nuclei such as ^{12}C and ^{16}O.[21,6] Greenlees *et al.*[22] were able to obtain much improved fits at backward angles by introducing a nonlocal term, which treats explicitly exchange, thus pointing out a way of improving the standard phenomenological optical model.

An improved fit to the 30.3-, 40.0-, and 61.4-MeV data was obtained by Sinha and Edwards[23] by the addition of a derivative Woods-Saxon term to the real central part of the optical potential. This

term represents the symmetry potential arising from the excess neutrons. It should be remarked, however, that the "half" radius of the symmetry term was found to be slightly larger than the one for the Woods-Saxon real central potential term. Secondly, one certainly expects the fits to the experimental data to improve considerably by the inclusion of additional parameters associated with the derivative term. In the present analysis no attempt was made to include such a derivative term because of the uncertainty already present in the spin-orbit parameters resulting from a lack of polarization data.

With the exception of a few cases, the normalization factor N^{-1} for the differential cross sections has a value much closer to 1.00 than what is expected from the experimental uncertainties in the absolute scales. This should not be surprising since, for all data below 100 MeV, N is determined at the end of a search as described previously.[7] For the data at 156, 160, and 185 MeV, however, it was found necessary to let the normalization factors vary more freely. One of the reasons for this was that with the method mentioned above it was impossible to get acceptable values for the diffuseness of the real central potential. The values obtained for the normalization factors of the latter data can be considered reasonable because after renormalization the angular distributions are very similar in shape and magnitude if plotted as a function of momentum transfer. One does not expect the magnitude of the differential cross sections to vary much between 156 and 185 MeV.

Due to restrictions in the computer time available, the 1.04-GeV data were analyzed without spin-orbit potential terms. The resulting fit is nevertheless quite good as seen in Fig. 1(d). However, as is evident from Table II, the radius parameter of the imaginary central potential is rather small compared to the values found at the other energies and is at this energy even smaller than the radius parameter of the real central potential.

The theoretical and experimental polarization angular distributions are shown in Fig. 2. Again the fits are quite good. Where high-precision differential cross-section and polarization data are available at the same energy, the optical model can give good fits to both angular distributions simultaneously. This is demonstrated in Figs. 1 and 2, for instance, by the fits to the 30.3-MeV data. The inclusion of polarization data was found to be particularly important at the higher energies. Thus in the analysis of the 160-MeV data the 185-MeV polarization data with 50% larger errors were used. As shown in Table II there is in general good agreement between the theoretical and experimental reaction cross sections. If the experimental reaction cross sections at the same or nearby energies are averaged then all theoretical reaction cross sections agree with the experimental ones within two standard deviations.

The strength parameters obtained in the "all parameter" fits show definite trends with energy very similar to the trends observed in the previous analysis[6,7] of the $p + {}^{16}O$ and $p + {}^{40}Ca$ data. The strength of the real central potential decreases slowly with increasing incident energy, while from 30 MeV on the strength of the volume part of the imaginary central potential increases slowly with increasing energy. The strength of the surface part of the imaginary central potential decreases slowly with energy. The geometrical parameters do not show any such distinct trends at variance with what was observed for the $p + {}^{40}Ca$ system.[7]

In order to determine the energy dependence of the strength of the real central potential a common geometry has to be established first. The geometrical parameters corresponding to the "all parameter" fits (including those for the higher-energy data) were averaged, resulting in the following "average" geometry:

$$r_0 = 1.183 \text{ fm}, \quad r_i = 1.273 \text{ fm}, \quad r_s = 1.160 \text{ fm},$$
$$a_0 = 0.724 \text{ fm}, \quad a_i = 0.699 \text{ fm}, \quad a_s = 0.677 \text{ fm}.$$

The average geometry parameters satisfy the relations $r_i > r_0 > r_s$ and $a_0 > a_i > a_s$. The values for r_0 and r_s are very close to what is expected for ^{208}Pb if the peaking of the spin-orbit interaction is to occur at the maximum in the nucleon density gradient.[24] The average geometry for $p + {}^{208}Pb$ differs somewhat in both the imaginary central potential and the spin-orbit potential from the average geometry of Fricke *et al.*[19] for $A > 28$ used in the energy range 30–60 MeV and of Becchetti and Greenlees[25] for $A > 40$ and $T_p < 50$ MeV. It can be noted that the average spin-orbit parameters ($V_s = 6.18$ MeV, $r_s = 1.160$ fm, $a_s = 0.677$ fm) are slightly different from the spin-orbit parameters used in the "all parameter" searches at the energies where no polarization data were available.

Although there might be some preference for the average spin-orbit parameters obtained in the present analysis, the lack of polarization data in the low-energy region makes it difficult to be very definitive. The differential cross-section angular distributions alone tend to require rather large values for a_s in order to considerably improve the fits to the backward part of the angular distributions. These large values for a_s are out of line with the values obtained when both differential cross-section and polarization data are fitted simultaneously. Consequently no attempt was made to obtain a new set of "all parameter" fits at ener-

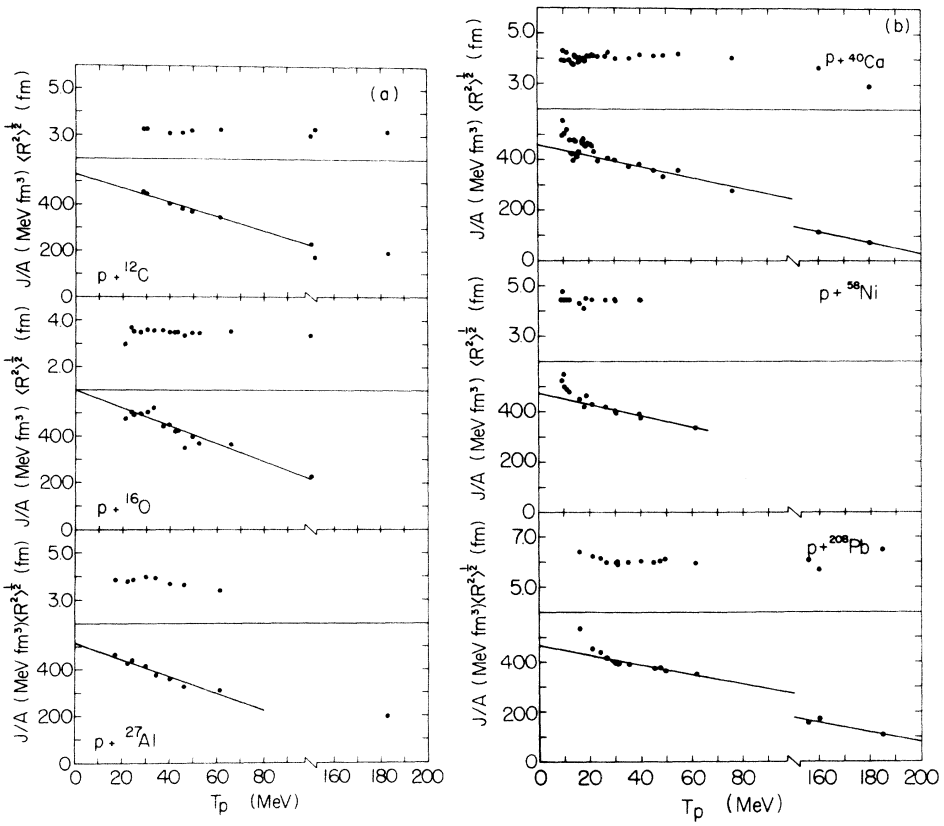

FIG. 3. (a), (b) The rms radius and the volume integral per nucleon of the real central optical potential plotted versus the incident proton energy for the range 0–200 MeV. The solid lines represent linear fits to the volume integrals per nucleon according to the relation $J/A = J_0/A + \alpha_J T_p$. Note the discontinuity in the abscissa. For numerical values of the quantities J_0/A and α_J see Table IV.

gies with no polarization data using the average spin-orbit parameters defined in the present analysis.

With the geometrical parameters fixed only five adjustable parameters were left to be determined, i.e., the five dynamical parameters V, W, W_D, V_S, and W_S. The same restrictions were made on the dynamical parameter searches as on the "all parameter" searches. The numerical values of the various potential strengths obtained in the searches with the average geometry are given in Table III. The same remarks as above can be made regarding the behavior of the dynamical parameters with energy.

An attempt was also made to analyze the 1.04-GeV data with the average geometry parameters. Without spin-orbit terms, however, the calculated values always fell considerably below the experimental data for the larger angles. By adding a real spin-orbit term in the potential the fit was considerably improved but then the calculated reaction cross section became much too small. It is interesting to note that in this calculation not only the real central potential but also the real spin-orbit term had a sign opposite to that found at lower energies. Even though it seems reasonable to assume that the addition of an imaginary spin-orbit term may give a more acceptable value for the reaction cross section it was not found worthwhile to perform further calculations without polarization data.

DISCUSSION

It has been shown that the rms radius and, to a lesser degree, the volume integral per nucleon of the real central potential are the well-defined quantities in optical-model analyses. The volume integral per nucleon and the rms radius are defined as:

$$J/A = \left[\int V(r)d^3r\right] \Big/ A = \frac{4\pi}{3} V r_0^3 \left(1 + \frac{\pi^2 a_0^2}{r_0^2 A^{2/3}}\right),$$

$$\langle R^2\rangle = \frac{\int r^2 V(r) d^3r}{\int V(r) d^3r} = \frac{1}{5}(3r_0^2 A^{2/3} + 7\pi^2 a_0^2). \qquad (4)$$

Both J/A and $\langle R^2\rangle^{1/2}$ calculated using the corresponding parameters of the real central potential

TABLE IV. Energy dependence of the volume integral per nucleon (J/A) and the strength of the real central part of the optical potential (V): $J/A = J_0/A + \alpha_J T_p$, $V = V_0 + \alpha_V T_p$. The values for α_V in the eighth column are due to Owen and Satchler for their force labeled "$E + 0$".

	Energy range (MeV)	J_0/A (MeV fm^3)	α_J (fm^3)	Energy range (MeV)	V_0 (MeV)	α_V	α_V force "$E + 0$"	References
$p + {}^{12}C$	25–100	530 ± 10	−3.03 ± 0.18					a
$p + {}^{16}O$	25–100	594 ± 25	−3.80 ± 0.50	20–100	60.7 ± 1.8	−0.37 ± 0.04	−0.301	b
$p + {}^{27}Al$	25–60	517 ± 26	−3.59 ± 0.61	20–60	57.1 ± 2.9	−0.37 ± 0.07		c
$p + {}^{40}Ca$	25–180	461 ± 6	−2.16 ± 0.07	20–180	55.4 ± 1.0	−0.28 ± 0.03	−0.267	d
$p + {}^{58}Ni$	25–60	469 ± 12	−2.14 ± 0.30					e
$p + {}^{208}Pb$	25–185	455 ± 3	−1.87 ± 0.03	20–185	62.4 ± 1.1	−0.30 ± 0.03	−0.202	Present work

[a] R. M. Craig, J. C. Dore, G. W. Greenlees, J. Lowe, and D. L. Watson, Nucl. Phys. 83, 493 (1966); R. C. Barrett, A. D. Hill, and P. E. Hodgson, *ibid.* 62, 133 (1965); Refs. 19 and 18; J. A. Fannon, E. J. Burge, D. A. Smith, and N. K. Ganguly, *ibid.* A97, 263 (1967); C. B. Fulmer, J. B. Ball, A. Scott, and M. L. Whiten, Phys. Rev. 181, 1565 (1969); T. Y. Li and S. K. Mark, Can. J. Phys. 46, 2645 (1968).

[b] References 6, 27, and 28.

[c] H. S. Sandhu, J. M. Cameron, and W. F. McGill, Nucl. Phys. A169, 600 (1971).

[d] Reference 7.

[e] Reference 19; D. L. Watson, J. Lowe, J. C. Dore, R. M. Craig, and D. J. Baugh, Nucl. Phys. A93, 193 (1967); Ref. 24; H. S. Liers, R. N. Boyd, C. H. Poppe, J. A. Sievers, and D. L. Watson, Phys. Rev. C 2, 1399 (1970); C. B. Fulmer, J. B. Ball, A. Scott, and M. L. Whiten, Phys. Lett. 24B, 505 (1967).

are given in Table II. Note that the rms radius is a constant for incident proton energies above 25 MeV. Below 25 MeV there is a small but definite trend towards larger values for decreasing incident energy. The same observation has been made by Makofske *et al.*[26] in comparing the results of optical-model analyses of proton scattering data at 9.8, 16.0, and 30.3 MeV. Similarly there is below 25 MeV a substantial increase in the volume integral per nucleon for decreasing incident proton energy. The significant increase in both quantities below 25 MeV may be attributed to effects due to core polarization and antisymmetrization not included in the standard optical model.[26]

The energy dependence of J/A for $p + {}^{12}C$, $p + {}^{16}O$, $p + {}^{27}Al$, $p + {}^{40}Ca$, $p + {}^{58}Ni$, and $p + {}^{208}Pb$ in the energy range 0–200 MeV is compared in Fig. 3. The optical-model parameters used in calculating J/A for $p + {}^{16}O$ and $p + {}^{40}Ca$ correspond to the "all parameter" fits of previous studies of the energy dependence.[6,7] In the case of $p + {}^{16}O$ additional optical-model analyses were made of the more recent data at 65.8[27] and 100 MeV.[28] The optical-model parameters used in calculating J/A for $p + {}^{12}C$, $p + {}^{27}Al$, and $p + {}^{58}Ni$ were adopted from the literature (see Table IV). The energy dependence of the real central potential is commonly presented by a linear relation in the incident proton kinetic energy. Excluding the results below 25 MeV, one finds that J/A exhibits a linear energy dependence ($J/A = J_0/A + \alpha_J T_p$) over a limited energy range. The energy range appears to increase somewhat with increasing A. The solid lines represent fits to the values of J/A according to the linear relation given above. The energy dependence is specified in Table IV. Secondly, one can remark that below 25 MeV there is in general a substantial increase in J/A for decreasing proton energy. As stated before, the significant increase in J/A may be attributed to effects due to core polarization and antisymmetrization not included in the standard optical model. In optical-model analyses of the light nuclei, like ^{12}C and ^{16}O, there are additional difficulties due to compound nucleus scattering and the existence of resonances in the intermediate compound system. Thus the values of J/A for incident proton energies below 25 MeV do not necessarily reflect the actual energy dependence of the optical potential. Finally there exists a marked decrease in the magnitude of α_J for increasing A. This decrease can only be partly explained as due to the A dependence of J/A as defined above.

Similar to J/A, one finds that the energy dependence of the strength of the real central potential can be represented by a linear relation ($V = V_0 + \alpha_V T_p$) over a limited energy range. A comparison of the energy dependence of V for $p + {}^{16}O$, $p + {}^{27}Al$, $p + {}^{40}Ca$, and $p + {}^{208}Pb$ is given in Table IV. It should be noted that the magnitude of α_V is decreasing for increasing A. A similar decrease in the magnitude of α_V was found by Owen and Satchler.[29] These authors treated exchange effects in nucleon-nucleus elastic scattering explicitly by us-

ing a nonlocal potential for the exchange term. The calculated values of α_V are somewhat smaller in magnitude than the empirical ones. There is therefore some indication that the energy dependence of the real central potential is not entirely due to the nonlocality of the optical potential. The same conclusion was reached by Slanina and McManus[30] who used in their calculations an equivalent local potential for the exchange term.

The large negative values of α_J or α_V cause the real central potential to change sign at relatively low energies in disagreement with the results of optical-model analyses[31] of proton scattering data at higher energies. Consequently the linear energy dependence determined for the low-energy region cannot be extrapolated to higher energies. In particular, if the energy range 25–1000 MeV is considered, then the empirical values of J/A tend to indicate a logarithmic energy dependence of the type $J/A = J_0/A + \beta_J \ln(T_p)$[32] as shown in Fig. 4 for the $p + {}^{208}$Pb system. Some evidence for a logarithmic energy dependence has been given by Passatore[5] as the asymptotic behavior at high energy. This follows from the assumption that the imaginary local optical potential approaches a constant value at high energy resulting in a logarithmic energy dependence of the leading term of the dispersion integral.

As also shown previously for the $p + {}^{40}$Ca system[7] the rms radius is constant over a considerable energy range. Excluding the values below 25 MeV for reasons discussed before, the average of all results gives $\langle R^2\rangle_{\rm opt}^{1/2} = 6.00 \pm 0.04$ fm. The rms radius of the real central potential was converted into a point-matter radius using the first-order relation given by Greenlees, Makofske, and Pyle[33]:

$$\langle R^2\rangle_m = \langle R^2\rangle_{\rm opt} - \langle R^2\rangle_d ,$$

where $\langle R^2\rangle_d$ is the rms radius of the nucleon-nucleon force. If a value of 4.27 fm^2 is chosen for $\langle R^2\rangle_d$ as suggested by Greenlees, Makofske, and Pyle[33] then $\langle R^2\rangle_m^{1/2} = 5.63$ fm. The rms radius for the charge distribution, which is obtained from electron scattering and μ-mesic x-ray studies, is $\langle R^2\rangle_{\rm ch}^{1/2} = 5.501$ fm.[34] This results in a rms radius of the proton distribution $\langle R^2\rangle_p^{1/2} = 5.44$ fm. Thus there is some evidence that the neutron distribution in ^{208}Pb extends outside the proton distribution. A similar conclusion was also reached following an analysis of (p, n) quasielastic scattering from ^{208}Pb.[35] The ratio of the rms radii for the neutron and proton distributions determined ($\langle R^2\rangle_n^{1/2}/\langle R^2\rangle_p^{1/2} = 1.07 \pm 0.03$) is in good agreement with the results of the present analysis.

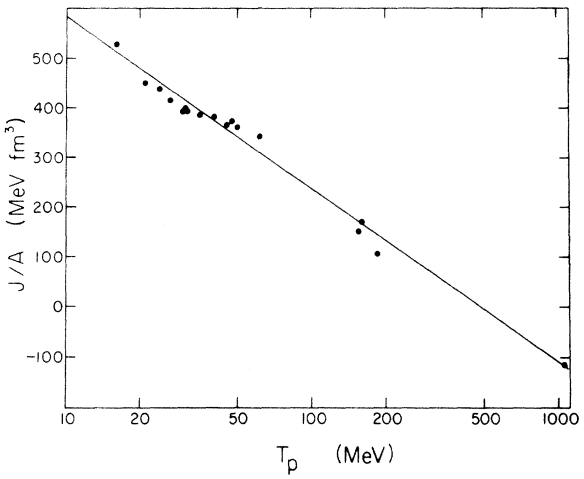

FIG. 4. The volume integral per nucleon of the real central optical potential plotted versus the incident proton energy for the range 10–1100 MeV. The solid line represents a logarithmic fit to the volume integral per nucleon according to the relation $J/A = J_0/A + \beta_J \ln(T_p)$.

*Work supported in part by the Atomic Energy Control Board of Canada and the Swedish Atomic Research Council.

[1]H. Feshbach, Ann. Phys. (N. Y.) 5, 357 (1958).
[2]R. Lipperheide, Z. Phys. 202, 58 (1967).
[3]R. Lipperheide and A. K. Schmidt, Nucl. Phys. A112, 65 (1968).
[4]H. Fiedeldey and C. A. Engelbrecht, Nucl. Phys. A128, 673 (1969).
[5]G. Passatore, Nucl. Phys. A96, 694 (1967); A110, 91 (1968).
[6]W. T. H. van Oers and J. M. Cameron, Phys. Rev. 184, 1061 (1969); in *Proceedings of the International Conference on Properties of Nuclear States*, edited by M. Harvey *et al.* (Presses de l'Université de Montréal, Montréal, 1969).
[7]W. T. H. van Oers, Phys. Rev. C 3, 1550 (1971).
[8]R. F. Carlson, private communication.
[9]A. Ingemarsson, The Gustaf Werner Institute Report No. GWI-PH 6/73 (unpublished).
[10]B. M. Bardin and M. E. Rickey, Rev. Sci. Instrum. 35, 902 (1964); R. Smythe, *ibid.* 35, 1197 (1964).
[11]H. Willmes, Nucl. Instrum. 41, 122 (1966); K. H. Bray, K. S. Jayaraman, G. A. Moss, W. T. H. van Oers, D. O. Wells, and Y. I. Wu, Nucl. Phys. A167, 47 (1971).
[12]L. H. Johnston, D. F. Service, and D. A. Swenson, IEE Trans. Nucl. Sci. 5, 95 (1958); D. F. Measday and R. J. Schneider, Nucl. Instrum. 42, 26 (1966); D. F. Measday and C. Richard-Serre, *ibid.* 76, 45 (1969).
[13]B. Höistad, A. Ingemarsson, A. Johansson, and G. Tibell, Nucl. Phys. A119, 290 (1968).
[14]M. A. Melkanoff, J. Raynal, and T. Sawada, University

of California at Los Angeles Report No. 66-10 (unpublished).
[15]W. R. Smith, Atlas Computer Laboratory, Nuclear Physics Programme Library Report No. 9, Los Angeles, February, 1967 (unpublished).
[16]A. Ingemarsson and G. Tibell, Physica Scripta 4, 235 (1971).
[17]R. Hofstadter, Annu. Rev. Nucl. Sci. 7, 231 (1957).
[18]G. R. Satchler, Nucl. Phys. A100, 497 (1967).
[19]M. P. Fricke, E. E. Gross, B. J. Morton, and A. Zucker, Phys. Rev. 156, 1207 (1967).
[20]R. R. Doering, A. J. Galonsky, and R. A. Hinrichs, Michigan State University, Cyclotron Laboratory Report No. MSUCL-61, 1972 (unpublished).
[21]J. Lowe and D. L. Watson, Phys. Lett. 23, 261 (1966); 24B, 174 (1967).
[22]G. W. Greenlees, W. Makofske, Y. C. Tang, and D. R. Thompson, Phys. Rev. C 6, 2057 (1972).
[23]B. C. Sinha and V. R. W. Edwards, Phys. Lett. 31B, 273 (1970).
[24]G. W. Greenlees, V. Hnizdo, O. Karban, J. Lowe, and W. Makofske, Phys. Rev. C 2, 1063 (1970).
[25]F. D. Bechetti and G. W. Greenlees, Phys. Rev. 182, 1190 (1969).
[26]W. Makofske, G. W. Greenlees, H. S. Liers, and G. J. Pyle, Phys. Rev. C 5, 780 (1972).
[27]G. M. Lerner and J. B. Marion, Nucl. Phys. A193, 593 (1972).
[28]A. Houdayer, T. Y. Li, and S. K. Mark, Can. J. Phys. 48, 765 (1970).
[29]L. W. Owen and G. R. Satchler, Phys. Rev. Lett. 25, 1720 (1970).
[30]D. Slanina and H. McManus, Nucl. Phys. A116, 271 (1968).
[31]P. G. McManigal, R. D. Eandi, S. N. Kaplan, and B. J. Moyer, Phys. Rev. 137, B620 (1965); H. Palevsky, J. L. Friedes, R. J. Sutter, G. W. Bennett, G. J. Igo, W. D. Simpson, G. C. Phillips, D. M. Corley, N. S. Wall, R. L. Stearns, and B. Gottschalk, Phys. Rev. Lett. 18, 1200 (1967); D. L. Hendrie, private communication.
[32]W. T. H. van Oers and Huang Haw, Phys. Lett. 45B, 207 (1973).
[33]G. W. Greenlees, W. Makofske, and G. J. Pyle, Phys. Rev. C 1, 1145 (1970).
[34]J. Heisenberg, R. Hofstadter, J. S. McCarthy, I. Sick, B. C. Clark, R. Herman, and D. G. Ravenhall, Phys. Rev. Lett. 23, 1402 (1969).
[35]S. D. Schery, D. A. Lind, and C. D. Zafiratos, Phys. Rev. C 9, 416 (1974).
[36]J. Raynal, Centre d'Etudes Nucléaires de Saclay, Report No. DPL-T/69-42 (unpublished).